Fabrication of Mesoporous Co_3O_4 from LP-FDU-12 via Nanocasting Route and Effect of Wall/Pore Size on Their Magnetic Properties

Hongxiao Jin,[†] Xiaojian Gu,[†] Bo Hong,*,[†] Langsheng Lin,[‡] Chiya Wang,[†] Dingfeng Jin,[†] Xiaoling Peng,[†] Xinqing Wang,[†] and Hongliang Ge[†]

[†]Zhejiang Province Key Laboratory of Magnetism, College of Materials Science and Engineering, China Jiliang University, Hangzhou 310018, People's Republic of China

[‡]High Magnetic Field Laboratory, Chinese Academy of Sciences, Hefei 230031, China

Ⓢ Supporting Information

ABSTRACT: Highly ordered mesoporous Co_3O_4 nanostructures were prepared using LP-FDU-12 as hard templates. By changing the hydrothermal temperature or by the acid treatment of the LP-FDU-12 template, Co_3O_4 replicas with different cell parameters and wall thicknesses have been obtained. The structure and textural characteristics of both LP-FDU-12 and Co_3O_4 replicas were investigated by X-ray diffraction, transmission electron microscopy, and N_2 adsorption−desorption isotherm analysis. The cell parameter and wall thickness of a mesoporous Co_3O_4 have been varied systematically within the ranges 30.4−33.9 and 24.8−18.2 nm, respectively, and the materials exhibit surface areas in the 29.6−52.9 m^2 g^{-1} range, while preserving a highly ordered 3D pore structure and highly crystalline walls. Most importantly, magnetic studies show that the factors which affect the magnetic behavior in the Co_3O_4 nanosphere system are not only the sphere size but also the space-filled parameter at the nanoscale.
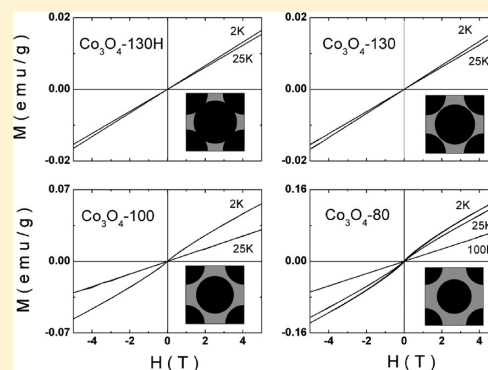
1. INTRODUCTION

Mesoporous Co_3O_4, which is among the most extensively studied oxides, is arousing increasing interest due to its potential applications in a variety of fields such as electrochemistry,[1−3] catalysis,[4,5] and magnetic storage devices.[6−10] Most familiarly, the mesoporous Co_3O_4 can be synthesized by hard templating, a method also called nanocasting,[11] from which the replica structures of mesoporous templates may be cast. The shape, size, and structure of mesoporous Co_3O_4 can be systemically engineered by controlling the morphology, the topology of the pores, and the pore size and wall thickness of the mesoporous hard template. The hard templating route has opened the way to great varieties of mesoporous Co_3O_4.[12] To date, various types of mesoporous silicas, such as SBA-15,[13−18] KIT-6,[14,16−19] SBA-16,[13,20,21] FDU-12,[21] and AMS-10[18] etc., were used as a hard template for synthesizing mesoporous Co_3O_4 with different pore symmetries. Among these, Co_3O_4 replicas of SBA-15 and KIT-6 have been extensively studied on both structural controlling and applications. Different from other known mesoporous materials, the replica of SBA-16[22] and FDU-12[23] (consisting of spherical nanocavities) could be regarded as 3D assemblies of nanospheres (the nanospheres connected to each other by some short nanorods to form a 3D arrangement[20,21]), which are potentially useful in studies of size-dependent optical, magnetic, and electrical transport properties of materials. The shape, size, and interparticle spacing of the assembly affected these properties deeply.

Therefore, syntheses that form controllable sizes and interparticle spaces are highly desirable.

Recently, magnetism of Co_3O_4 mesoporous structure has attracted much attention because the mesoporous structure alters the magnetic properties. Bulk Co_3O_4 has a spinel structure with Co^{3+} ions occupying the B sites (octahedral) and the Co^{2+} ions occupying the A sites (tetrahedral) and is antiferromagnetic (AFM) below 40 K, whereas it is paramagnetic (PM) above that temperature.[24,25] However, the magnetic measurements of mesoprous Co_3O_4 samples show that the magnetic behaviors are mainly effected by uncompensated surface spins. Mesoporous Co_3O_4 samples were prepared using SBA-15,[8,9,26] KIT-6,[7,9,10,27,28] and SBA-16[21,28] as hard silica templates and have been studied using magnetometry. In these studies, different types of mesoporous silicas were used as a hard template for the syntheses: the Co_3O_4 replica of SBA-15 consists of nanowires with an average diameter of about 8 nm and the nanowires surface disorder the exchanges bias field changes systematically.[8] A Co_3O_4 replica of KIT-6 has a bimodal pore system with columnlike walls and a pore size distribution centered at 40 and 90 Å.[10] The Co_3O_4 replica of SBA-16 consists of nanospheres connected by rods, and the diameter of the spheres is 10−12 nm.[21] From a comparative study on KIT-6 and SBA-16, it was observed that

the magnetization increases with a greater breakdown of long-range crystallographic ordering.[28]

The structure of the pores, the pore size, and the wall thickness of the mesoporous hard template affect the magnetic properties of Co_3O_4 mesoporous structure deeply. The relationship between the pore sizes and the wall thickness of the mesoporous Co_3O_4 and their magnetic properties are still interesting topics. Herein, the cubic mesostructure LP-FDU-12 that possesses a cage type pore system with a large spherical pore has been selected for studying the relationships. The dependence of the structure of replicas on pore size of the silica template and of the magnetic property on the wall thickness of Co_3O_4 will be discussed. Different from earlier literature, in this study, we focused on a comparative magnetic study on Co_3O_4 replicas with similar pore topology but different pore sizes and wall thicknesses.

2. EXPERIMENTAL SECTION

2.1. Materials. Tetraethyl orthosilicate (TEOS) (99%), 1,3,5-trimethylbenzene (TMB), potassium chloride (KCl), hydrochloric acid (HCl), sulfuric acid (H_2SO_4), and cobaltous nitrate [$Co(NO_3)_2\cdot 6H_2O$] were purchased from Shanghai Chemical Reagent Factory of China without further treatment. Triblock copolymer poly(ethylene oxide)-b-poly(propylene oxide)-b-poly(ethylene oxide) Pluronic F127 ($EO_{106}PO_{70}EO_{106}$, MW = 12600) was purchased from Aldrich. Distilled water was used in all experiments.

2.2. Synthesis of LP-FDU-12 Silica. The synthesis of mesoporous silica LP-FDU-12 has been reported previously by Fan and co-workers.[29] A typical synthesis was as follows: 4.0 g of F127, 4.8 g of TMB, and 20 g of KCl were dissolved in 240 mL of H_2O and 50 mL of HCl at 15 °C. After 6 h of stirring, 20 mL of TEOS was added to this solution. After further stirring for 20 h, the mixture was transferred into an autoclave and heated at the desired temperature for 24 h. As-made products were obtained by filtration and dried at room temperature in air. The silicas were calcined at 450 °C for 6 h with a ramp 5 °C min^{-1}. Calcined silica samples were designated as FDU-12-x, where x stands for the hydrothermal aging temperature applied during synthesis. To achieve less shrinkage pore structure,[30] the 130 °C hydrothermal treated sample was also refluxed in 4 M H_2SO_4 for 20 h to remove the template. This sample was designated as FDU-12-130H.

2.3. Preparation of the Mesoprous Co_3O_4. In a typical synthesis of mesoporous Co_3O_4, 6.0 g of $Co(NO_3)_2\cdot 6H_2O$ was dissolved in 30 mL of ethanol followed by the addition of 2 g of mesoporous silica template. The mixture was stirred at room temperature until a nearly dry powder had been obtained; the sample was then heated slowly to 200 °C and calcined at the same temperature for 6 h to pyrolyze the nitrate. The result material was reimpregnated again with 4.3 g of Co-$(NO_3)_2\cdot 6H_2O$ dissolved in 30 mL of ethanol, followed by calcination at 450 °C for 6 h with a ramp 1 °C min^{-1} for metal oxide to crystallize. The resulting sample was twice treated with a hot 2 M NaOH solution to remove the silica template, followed by washing with water and ethanol several times, and then drying at 60 °C. They were denoted as Co_3O_4-80, Co_3O_4-100, Co_3O_4-130, and Co_3O_4-130H in accordance with the assignment of hard templates.

2.4. Characterization. The mesostructures of LP-FDU-12 and Co_3O_4 were monitored by low-angle X-ray diffraction (XRD) and recorded on a Siemens D8 Advance diffractmeter with Ni-filtered Cu Kα radiation. Using wide-angle XRD, the

pure Co_3O_4 spinel phase was verified after NaOH etching. Transmission electron microscopy (TEM) experiments were conducted on a JEOL-JEM-2010 microscope operated at 200 kV. Nitrogen physisorption experiments were measured at 77 K on a nitrogen adsorption apparatus (ASAP 2020) after degassing samples at 180 °C for 5 h. The Brunauer−Emmett−Teller (BET) surface area (S_{BET}) was estimated using adsorption data in a relative pressure range from 0.04 to 0.3. The mesopore size distributions (PSD) were calculated by analyzing the adsorption data of the N_2 isotherm using the Barrett−Joyner−Halenda (BJH) method. The magnetic properties were measured by using a Superconducting Quantum Interference Device (SQUID) MPMS system under a 0.005 T magnetic field. The samples were first cooled down to 4 K without any external magnetic field, then M−T measurements were performed with warming to 300 K at a 0.005 T field. The FC curve was obtained after the temperature was reduced to 4 K at 0.005 T field and then measured with heating up to 300 K at the same magnetic field. The M−H hysteresis loops were measured with a field sweep from 5 to −5 T at different temperatures.

3. RESULTS AND DISCUSSION

3.1. Structure of Template. LP-FDU-12 materials were prepared according to the procedure of Fan et al.[29] As discussed elsewhere, the pore diameter of LP-FDU-12 can be adjusted by selecting the aging temperature and by subsequently acid treatment.[29−31] Four LP-FDU-12 samples with different pore sizes were synthesized for further incorporation of Co_3O_4. XRD powder patterns of the four samples (Figure S1 in the Supporting Information) represent two intensive well-resolved peaks in the region of $2\theta = 0.45-1.3°$, which can be indexed as the [111] and [311] reflections of a face centered cubic structure with space group $Fm\bar{3}m$ symmetry based on extensive investigations in the previous literature.[32,33] In the LP-FDU-12-80, LP-FDU-12-100, and LP-FDU-12-130 samples, which synthesized at aging temperatures of 80, 100, and 130 °C, respectively, an increase of the unit cell parameters with the aging temperature increase is observed (Table 1) from the fact that the [111] reflection peak shifts to a

Table 1. Structural Properties of Calcined Mesoporous Silica LP-FDU-12-X Samples[a]

sample	S_{BET} (m² g⁻¹)	V_T (cm³ g⁻¹)	d_0	a_0
			nm	
FDU-12-130H	614.6	0.967	17.8	34.6
FDU-12-130	520.2	0.611	15.6	33.2
FDU-12-100	369.0	0.496	13.1	33.2
FDU-12-80	349.5	0.336	12.2	29.4

[a]S_{BET} is the specific surface area deduced from the isotherm analysis in the relative pressure range of 0.05-0.2; V_T is the total pore volume at relative pressures 0.95; d_0 is the pore diameter calculated from the desorption branch of the isotherm using the BJH method; and the XRD unit cell parameter a_0 is equal to $3^{1/2}d_{111}$.

smaller angle, in agreement with literature reports.[31] In addition, for the LP-FDU-12-130H sample, which was synthesized at an aging temperature of 130 °C and subsequently treated with H_2SO_4, the unit cell parameters increased further, which was consistent with the observation of Yang et al.[30] TEM images (Figure S2 in the Supporting Information) of the representative sample (LP-FDU-12-100)

reveal that the materials possess 3D cubic mesoscopic order, in accord with the XRD patterns.

Nitrogen adsorption and desorption isotherms (Figure S3 in the Supporting Information) for the calcined LP-FDU-12-X samples are of type IV according to the IUPAC classification. The broad H2 type hysteresis loops characteristic for large cagelike mesopores are observed for all isotherms, indicating that entrances are much narrower than the pore cage diameter in the materials. A sharp capillary condensation step is registered in the relative pressure range of 0.80−0.90 depending on the material, indicating the presence of uniform mesopores with a narrow pore size distribution. A steep capillary evaporation step is located at the lower limit of adsorption−desorption hysteresis in the relative pressure range of 0.40−0.70, indicating that the entrances to the mesopores had diameters below 5 nm. All of the results are similar to LP-FDU-12 prepared under similar conditions by Fan et al.[29] and Kruk et al.[31] The specific BET surface area, pore volumes, and mean pore diameters of the samples are listed in Table 1. The pore size distribution curves, BJH plots of derivative of the pore volume per unit weight with respect to the pore diameter (dV/dD) versus the pore diameter (D), show a clear shift of pore diameter from 12.2 to 17.8 nm as the aging temperature is increased from 80 to 130 °C or by acid treatment.

3.2. Structure of Co_3O_4. Above-described LP-FDU-12 samples were then used as templates for the preparation of nanostructured Co_3O_4 spinels. In a general preparation procedure of nanocast Co_3O_4, 3D cubic LP-FDU-12 templates are impregnated with a solution of cobalt nitrate in ethanol, calcined, and eventually reimpregnated to maximize the loading with inorganic precursor. To recover the mesoscaled Co_3O_4, we dissolved the parent silica templates with hot 2 M NaOH solution. The remaining materials consist of ordered sphere arrays, which reflect the pore topology of the parent material. Figure 1 shows the TEM images of the Co_3O_4 mesoporous replicas synthesized with FDU-12-130H sample after NaOH etching. Nanoshperes of Co_3O_4 with a diameter of about 24 nm were assembled into microparticles with size of several micrometers. These values are comparable with the particle size for Co_3O_4 sample reported by Yue et al.[21,34] From HR-TEM (Figure 1c), it can be seen that the spheres are crystalline,

and each of them can be regarded as a single crystal, although the crystal orientations of the two adjacent Co_3O_4 nanospheres are different. Some irregular bubbles like spherical mesopores are also found in the image. This probably related with an in situ $Co(NO_3)_2 \cdot 6H_2O$ to Co_3O_4 conversion and ripening under high temperature: thermal decomposition of $Co(NO_3)_2 \cdot 6H_2O$ to Co_3O_4 would leave some micropores due to the shrinkages in volume, and under heating, an in situ ripening of the neighboring Co_3O_4 around the micropores to minimize the surface energy; as a result, bubbles like spherical mesopores formed. The corresponding wide-angle XRD patterns are shown in Figure 2, which can be perfectly indexed to cubic spinel Co_3O_4 (JCPDS card no. 42-1467; space group, $Fd\bar{3}m$; a_0 = 8.084 Å) and consistent with the TEM data. No indication of cobalt silicates was observed in XRD analysis, and energy dispersive X-ray (EDX) analysis proved the removal of silicate down to trace levels (<1%). All of the other three Co_3O_4 have identical XRD patterns (Figure S4 in the Supporting Information) and resemble EDX results (not shown), suggesting that the Co_3O_4 products are pure and well-crystalline.

All of the Co_3O_4 mesoporous replicas were analyzed with TEM, nitrogen physisorption, and wide- and low-angle XRD measurements. Table 2 summarizes the structural properties of the mesoporous Co_3O_4-X.

Figure 3 shows the low-angle XRD of the mesoporous Co_3O_4 after dissolution of the silica. Only one reflection peak with high intensity within the range of 0.6−3.0 (2θ) is observed from each pattern, which can be assigned to the [111] reflections of an fcc structure ($Fm\bar{3}m$). The cell parameters (a) are calculated to be 33.5, 33.2, 31.5, and 30.4 nm for Co_3O_4-130H, Co_3O_4-130, Co_3O_4-100, and Co_3O_4-80, respectively, showing the d-spacing a little smaller than that of the corresponding mother silica template, suggesting complete replicate of the templates. The lattice parameters exhibit the same trend as for the silica for samples Co_3O_4-80, Co_3O_4-100, and Co_3O_4-130, increasing with increasing temperature. The cell parameter of Co_3O_4-130H is larger than that of Co_3O_4-130 due to less shrinkage of the template being used.

Figure 4 shows the nitrogen adsorption−desorption isotherms of the porous Co_3O_4 products. The isotherms of Co_3O_4 porous crystals are all type IV with a typical H1 hysteresis loop of metal oxides prepared by hard-templating method. The specific surface areas of Co_3O_4-130H, Co_3O_4-130, Co_3O_4-100, and Co_3O_4-80 are 43.1, 52.9, 29.6, and 37.0 m² g⁻¹, respectively, which are smaller than the surface area of Co_3O_4 templated by KIT-6,[14] SBA-15,[13] SBA-16,[16] AMS-10,[18] and small pore FDU-12.[21] Such differences are inherited from the large pore, with a thin wall FDU-12 being used as the template in the current syntheses; as a result, the Co_3O_4 replicas are of small pore, thick pore wall, and relatively low surface area. The micropore volumes are quite significant (0.011−0.021 cm³ g⁻¹), and the pore volume shifts from 0.085 to 0.223 as the different template is used. The average pore sizes of the Co_3O_4 replicas resemble each other with a size around 8.2 nm, implying that a change of aging temperature in the template synthesis or acid treatment of the template have little effect in the wall thickness and the subsequent adjustment of pore size of Co_3O_4 replicas. On the other hand, the increase of cell parameter from Co_3O_4-80 to Co_3O_4-130H as shown by XRD results in combination of which the N_2 adsorption−desorption characterization results suggest that the wall thickness (or sphere diameter) of the Co_3O_4 replicas could be readily adjusted because the pore size
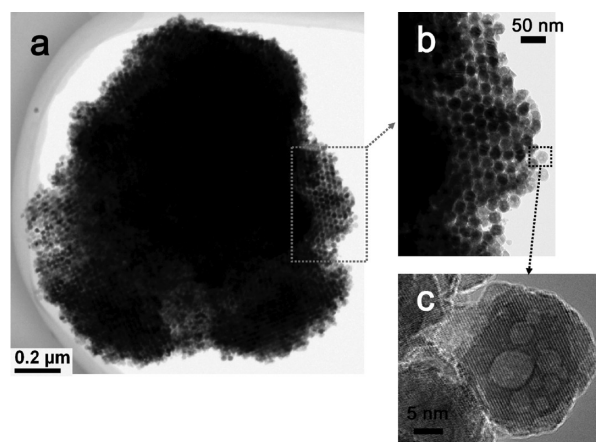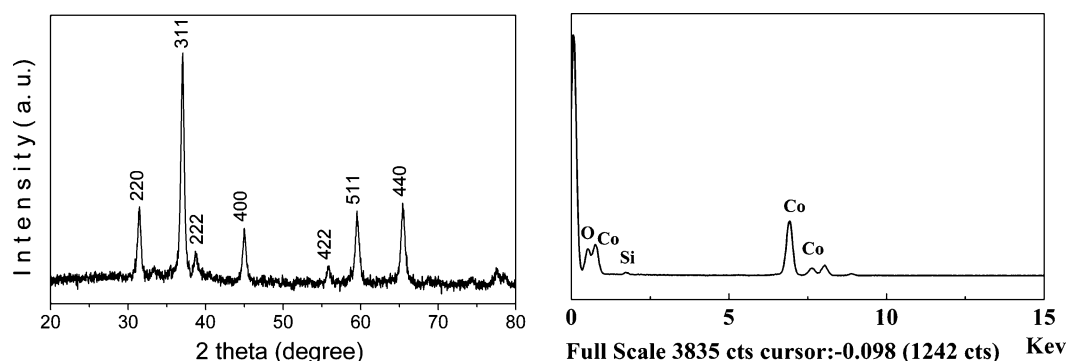

Figure 1. Interconnectivity and mesoporous ordered domain size. TEM and HR-TEM images of nanocast Co_3O_4-130H templated by FDU-12-130H: (a) low magnitude show particle size of 1−2 μm, (b) higher magnitude of a selected area in panel a, and (c) HR-TEM of a selected area in panel b.

Figure 2. Left: Wide-angle powder XRD pattern for the mesoporous Co_3O_4-130H sample. Right: EDX analyses of the mesoporous Co_3O_4-130H sample.

Table 2. Structural Properties of the Mesoporous Co_3O_4 Replicas[a]

	$m^2\,g^{-1}$	$cm^3\,g^{-1}$		nm			
sample	S_{BET}	V_T	V_{mi}	d_0	a_0	D_w	V_{occ}
Co_3O_4-130H	43.1	0.131	0.021	8.2	33.9	24.8	0.818
$Co3O4$-130	52.9	0.223	0.033	8.3	33.2	22.4	0.641
Co_3O_4-100	29.6	0.085	0.011	8.1	31.5	19.8	0.518
Co_3O_4-80	37.0	0.125	0.018	8.3	30.4	18.2	0.448

[a]S_{BET} is the specific surface area deduced from the isotherm analysis in the relative pressure range of 0.05−0.2; V_T is the total pore volume at relative pressures 0.95; V_{mi} is the micropore volume determined using the α_s plot method; d_0 is the pore diameter calculated from the desorption branch of the isotherm using the BJH method; the XRD unit cell parameter a_0 is equal to $3^{1/2}d_{111}$; D_w is the sphere diameter of the wall measured from TEM; and V_{occ} is a space-filled parameter, for spheres with a diameter of D_w stacking in a cubic with an edge size of a_0 in fcc symmetry, the space filling of the sphere could be expressed as follows:

$$V_{occ} = \frac{2}{3}\pi\left(\frac{D_w}{a_0}\right)^3$$

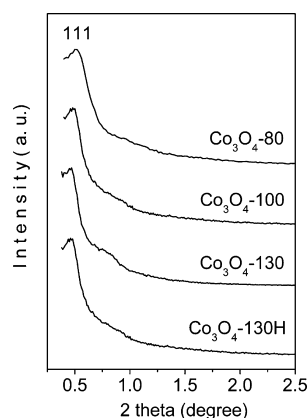**Figure 3.** Low-angle powder XRD patterns for the cubic mesoporous samples Co_3O_4-130H, Co_3O_4-130, Co_3O_4-100, and Co_3O_4-80.

of the mother template had been adjusted well. These results from XRD and N_2 adsorption−desorption are supported by TEM analysis.

TEM images of the obtained Co_3O_4 materials after NaOH etching are shown in Figure 5. In all cases, nanospheres of Co_3O_4 were observed. The average sphere size, which reflects the pore size of the parent silica matrix, is measured to be 24.8,

22.4, 19.8, and 18.2 nm for samples Co_3O_4-130H, Co_3O_4-130, Co_3O_4-100, and Co_3O_4-80, respectively. The TEM images clearly show the dependence of the sphere size of the resulting Co_3O_4 on the pore size of the parent silica, further corroborating the conclusion derived from XRD patterns and N_2 adsorption−desorption measurement. As reported by Yue et al.,[20,21] the nanospheres are connected by nanorods to prevent collapsing of the 3D structure, especially in cases where the cell parameters are larger than the size of two spheres (see the illustrative sample in Figure S5 in the Supporting Information). Examination of many different particles throughout each material suggests that the mesoporous structures replicate that of the hard template FDU-12-X, with space group of $Fm\bar{3}m$. Parts e−h in Figure 5 show TEM images and Fourier diffractograms (inset) of Co_3O_4-130H, Co_3O_4-130, Co_3O_4-100, and Co_3O_4-80, respectively, taken with [100], [311], [110], and [111] incidences, which is the same as that for LP-FDU-12[29] and KIT-5.[35] More TEM images are shown in Figure S6 in the Supporting Information, suggesting that the particles are several micrometers in size, which are composed of nanospheres.

3.3. Magnetic Properties. The cell parameters and walls size (spheres size) of the Co_3O_4 replicas are finely fabricated. Therefore, we can discuss the effect of these parameters on the magnetic properties of these samples. The temperature dependence of the magnetization (M−T) in a weak applied field of 50 Oe is shown in Figure 6. In the field-cooled (FC) measurements, the samples were cooled from 300 to 5 K in an external field of 50 Oe, while in the zero-field-cooling (ZFC) measurements, they were cooled under zero external field, and for both measurements, the magnetization was recorded on warming in a field of 50 Oe. For sample Co_3O_4-130H, a remarkable feature of the FC curve is the broad peak around 35 K, which corresponds to the AFM transition. This Néel temperature (T_N) is slightly lower than the bulk Co_3O_4, which has also been reported by other groups.[10] When the temperature is lower than T_N, first, the magnetization is decreased with the temperature decreases, and then, the value of M slightly rose below the temperature of 13 K, which may be attributed to a few surface spins arrangement consistent with the measurement field because of the thermal disturbance weakened. For sample Co_3O_4-130, its M−T behaviors are similar to that of the sample Co_3O_4-130H. However, for sample Co_3O_4-100, there is only an inflection and no obvious peak at 35 K in the M−T curve, and below 35 K, the increase of M is faster than that of samples Co_3O_4-130 and Co_3O_4-130H. For sample Co_3O_4-80, the rapid rise of M is observed below 50 K, especially the M rapid increase in the FC curve, and it decreases
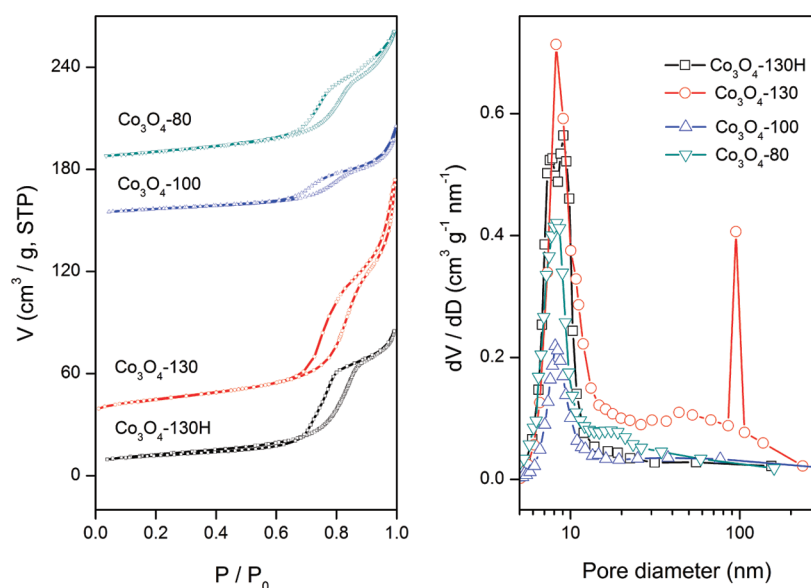
Figure 4. Nitrogen physisorption and pore size distributions for the mesoporous Co_3O_4 replicas templated by FDU-12-X. The isotherms of Co_3O_4-100, Co_3O_4-130, and Co_3O_4-130H were given with an offset of 30, 150, and 180 cm^3 g^{-1}, respectively.
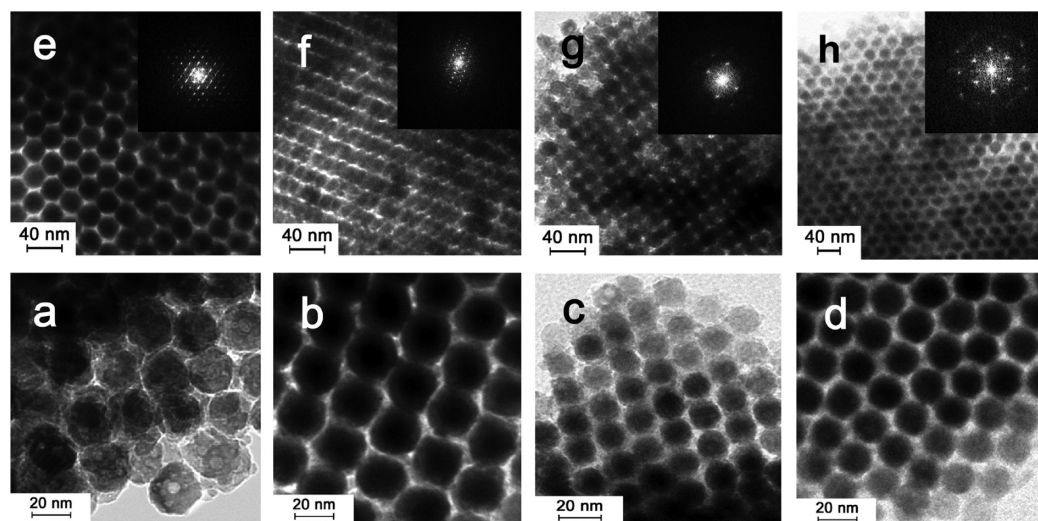

Figure 5. TEM images of mesoporous Co_3O_4 replicas, (a and e) Co_3O_4-130H, (b and f) Co_3O_4-130, (c and g) Co_3O_4-100, and (d and h) Co_3O_4-80. The insets in e−h are Fourier diffractograms from the corresponding TEM image, showing [100], [311], [110], and [111] incidences, respectively.

in the ZFC curve with the temperature decreasing at the low temperature. This obvious λ type irreversibility between the ZFC and the FC M−T curves implies the existence of clusterlike spin glass (SG).[36]

To make clear the different magnetic behavior in Co_3O_4 samples, measurement of the magnetization as a function of the magnetic field is performed at selected temperatures for all of the samples (Figure 7). For Co_3O_4-130 and Co_3O_4-130H samples, the M−H curves mostly behave linearly at $T < 25$ K, which indicate that there no FM phase in those samples. However, for the sample Co_3O_4-80, the M−H curve is not linear at $T < 25$ K; the obvious hysteresis loop is observed at the temperature 2 K, which is the unambiguous FM signal. The rapid increase of magnetization in Figure 6 originates from few FM coupling formation at low temperatures in Co_3O_4-80 sample, because the saturated value of M in the Co_3O_4-80 sample is much smaller than that in the usual FM system. For sample Co_3O_4-100, the M−H curve is not linear in the low

field, and the hysteresis loop at the temperature 2 K can not be found, which indicates that the FM coupling in sample Co_3O_4-100 is much less than that in sample Co_3O_4-80.

It is known that the magnetic behavior of bulk Co_3O_4 is AFM in the low temperature,[24,25] and the Néel temperature is about 40 K. Also, in some highly ordered Co_3O_4 nanoporous structures, the AFM phase is also observed at the low temperature, while its Néel temperature is lower than that of bulk Co_3O_4 because of the finite-size effect.[9,28,37] However, the obvious FM phases exist at the low temperature in some monodespersed Co_3O_4 nanorod.[8] Those phenomena all seem to be due to the size effects. However, in our samples, the magnetic behavior is much different at the low temperature (the clear AFM transform exists at 35 K for Co_3O_4-130 and Co_3O_4-130H samples, and for Co_3O_4-100 samples, this AFM transform is not obvious at 35 K, and there is no detectable AFM transform, but there are some FM phases at low temperatures for the Co_3O_4-80 sample). The differences in
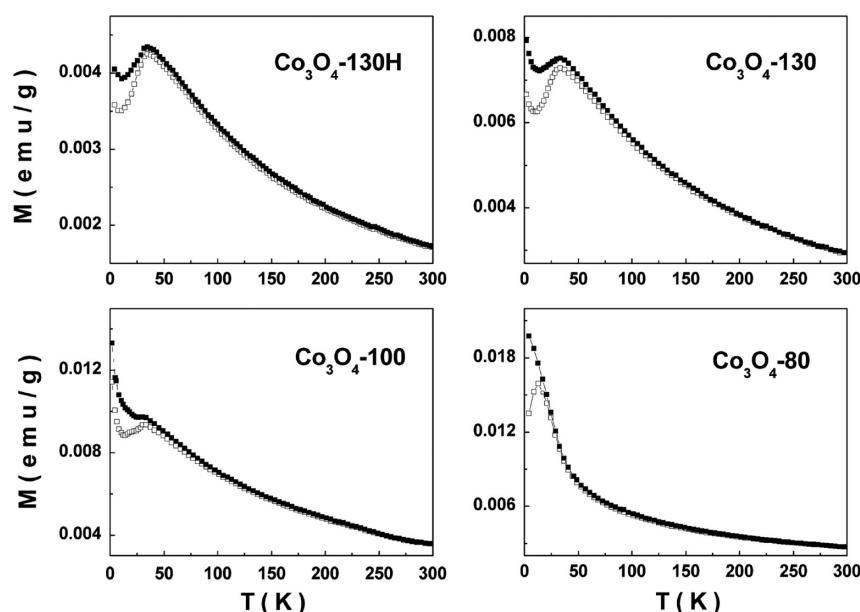
Figure 6. Temperature dependence of the magnetization for Co_3O_4 replicas. The open and solid squares represent zero-field cooling data and field cooling data, respectively.
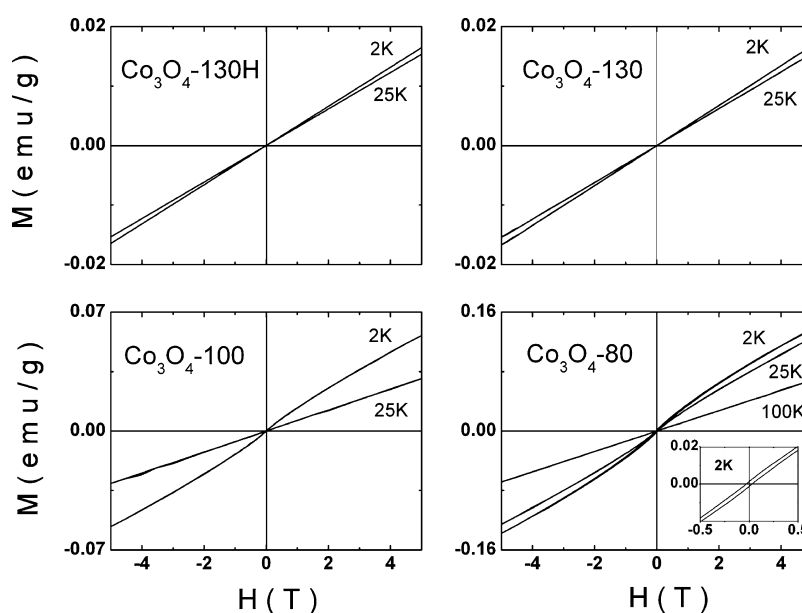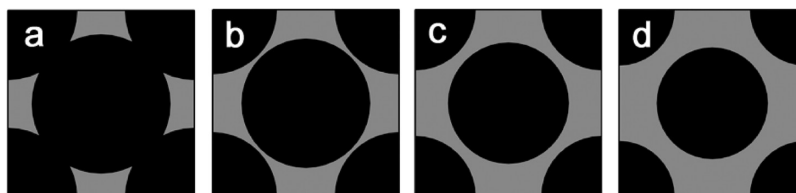

Figure 7. Magnetization as a function of the applied magnetic field for Co_3O_4 replicas.

Scheme 1. Schematic Drawing of the [100] Face of the Co_3O_4 Replicas with Different Space-Filled Parameters[a]

[a](a) Co_3O_4-130H, V_{occ} = 0.818; (b) Co_3O_4-130, V_{occ} = 0.641; (c) Co_3O_4-100, V_{occ} = 0.518; and (d) Co_3O_4-80, V_{occ} = 0.448. The space-filled parameter is defined in Table 1. The nanorods that support the nanospheres from collapsing are eliminated for clarity in b−d.

sphere sizes (18.2−24.8 nm) of our samples do not sufficiently support the changing of magnetic properties merely in considering the finite-size effect, and all samples are the Co_3O_4 and the face-centered cubic stacking; the material itself should make no difference. On the other hand, there are numerable nanorods smaller than 5 nm, which randomly connect the spheres to prevent the mesoporous structure from collapsing; they may cause reduction of the T_N. However, these

13379

dx.doi.org/10.1021/jp300645c | J. Phys. Chem. C 2012, 116, 13374−13381

nanorods are randomly distributed in all samples except Co_3O_4-130H, and the effect of those nanorods on all of these samples should be consistent. Therefore, there must be some other factors that change the magnetic properties. During careful analysis of synthesis and structural data, we notice that the value of its space-filled parameter (V_{occ} in Table 1) is a big difference in the samples. The V_{occ} values of the samples Co_3O_4-130H, Co_3O_4-130, Co_3O_4-100, and Co_3O_4-80 are 0.818, 0.641, 0.518, and 0.448, respectively, and the highest theoretically possible value of its space-filled parameter is 0.740. A schematic drawing of the [100] face of the Co_3O_4 replica with different V_{occ} is shown in Scheme 1. For the Co_3O_4-130H sample, the V_{occ} value is 0.818, which is more than the highest theoretically possible value 0.740. It means that Co_3O_4 spheres overlap each other; therefore, the obvious AFM phase exists at a low temperature in this sample, just like the behavior of the bulk Co_3O_4. With the decrease of V_{occ}, the AFM phase is gradually weakened, and the PM phase is gradually strong at the low temperature; indeed, the very few FM coupling appears at a temperature below 30 K in the Co_3O_4-80 sample. These phenomena indicate that the AFM behavior is suppressed and it will be conducted to the production of FM coupling in some small region with the increase of the distance between the spheres at low temperature. Until in some monodespersed Co_3O_4 nanorod, the obvious FM phases exist.[8]

As shown above, the V_{occ} value and the sphere size affect the magnetic property of the Co_3O_4 replicas systematically by changing the surface spins coupling between the spheres and the surface spins number. However, these interpretations are apparent; the true origin of the varying of the magnetic property of the Co_3O_4 replicas still needs to be further studied.

4. CONCLUSIONS

Face centered cubic ordered mesoporous Co_3O_4 samples have been prepared via the nanocasting route. The sphere size and distance between the spheres of the replicas are finely tailored for the first time by finely tuning the pore diameter and wall size of the template. It was demonstrated that the sphere diameter (wall thickness) and the distance between the spheres (pore size) in the mesoporous Co_3O_4 can be varied systematically within the range of 18.2−24.8 nm and 12.2 to 9.1 nm. The size of the nanospheres is larger than all of the previous reports on Co_3O_4 replicas from cage type mesoporous silica as a template due to LP-FDU-12 being used as a template in this study. The replicas show ordering from subnanometer size to micrometer size: (1) the walls are highly crystalline; (2) a highly ordered 3D pore structure is observed; and (3) the particles are several micrometers in size, which are composed of nanospheres.

We have also studied the magnetic behavior in highly ordered mesoporous Co_3O_4 nanostructures system by using the temperature dependence of the magnetization and the applied magnetic field dependence of the magnetization. On the basis of our experimental data, we suggest that the factors that affect the magnetic behavior in our Co_3O_4 nanosphere system are not only the size effect but also the space-filled parameter at the nanoscale, and the true origin of these behaviors needs further study.

The metal oxide replicas from cage type mesoporous material can be regarded as 3D assemblies of nanospheres, which are potentially useful in many fields. Various kinds of metal oxides can be synthesized in similar way. To obtain materials with

"target" optical, magnetic, and electronic properties, it is of crucial importance to vary the sphere distance and size. The results reported herein and their envisioned extensions open new opportunities in the development of 3D assemblies of nanospheres.

■ ASSOCIATED CONTENT

⑤ Supporting Information

Low-angle XRD patterns, TEM images, and nitrogen physisorption and pore size distributions for calcined mesoporous silica LP-FDU-12 samples, wide-angle powder XRD patterns, and TEM images of the mesoporous Co_3O_4 samples. This material is available free of charge via the Internet at http://pubs.acs.org.

■ AUTHOR INFORMATION

Corresponding Author
*Tel: +86-571-8687-5600. Fax: +86-571-8687-5600. E-mail: Bohong@cjlu.edu.cn or hongbo@mail.ustc.edu.cn.

Notes
The authors declare no competing financial interest.

■ ACKNOWLEDGMENTS

■ REFERENCES

(1) Zheng, M. B.; Cao, J.; Liao, S. T.; Liu, J. S.; Chen, H. Q.; Zhao, Y.; Dai, W. J.; Ji, G. B.; Cao, J. M.; Tao, J. *J. Phys. Chem. C* **2009**, *113*, 3887−3894.
(2) Xia, X.-H.; Tu, J.-P.; Wang, X.-L.; Gu, C.-D.; Zhao, X.-B. *Chem. Commun.* **2011**, *47*, 5786−5788.
(3) Cheng, F.; Tao, Z.; Liang, J.; Chen, J. *Chem. Mater.* **2008**, *20*, 667−681.
(4) Eggenhuisen, T. M.; den Breejen, J. P.; Verdoes, D.; de Jongh, P. E.; de Jong, K. P. *J. Am. Chem. Soc.* **2010**, *132*, 18318−18325.
(5) Jiao, F.; Frei, H. *Angew. Chem., Int. Ed.* **2009**, *48*, 1841−1844.
(6) Benitez, M. J.; Petracic, O.; Salabas, E. L.; Radu, F.; Tuysuz, H.; Schuth, F.; Zabel, H. *Phys. Rev. Lett.* **2008**, *101*, 097206.
(7) Benitez, M. J.; Petracic, O.; Tuysuz, H.; Schuth, F.; Zabel, H. *Phys. Rev. B* **2011**, *83*, 134424.
(8) Salabas, E. L.; Rumplecker, A.; Kleitz, F.; Radu, F.; Schuth, F. *Nano Lett.* **2006**, *6*, 2977−2981.
(9) Wang, G. X.; Liu, H.; Horvat, J.; Wang, B.; Qiao, S. Z.; Park, J.; Ahn, H. *Chem.—Eur. J.* **2010**, *16*, 11020−11027.
(10) Wang, Y. Q.; Yang, C. M.; Schmidt, W.; Spliethoff, B.; Bill, E.; Schuth, F. *Adv. Mater.* **2005**, *17*, 53−56.
(11) Lu, A. H.; Schuth, F. *Adv. Mater.* **2006**, *18*, 1793−1805.
(12) Yue, W. B.; Zhou, W. Z. *Prog. Nat. Sci.* **2008**, *18*, 1329−1338.
(13) Tian, B. Z.; Liu, X. Y.; Yang, H. F.; Xie, S. H.; Yu, C. Z.; Tu, B.; Zhao, D. Y. *Adv. Mater.* **2003**, *15*, 1370−1374.
(14) Dickinson, C.; Zhou, W. Z.; Hodgkins, R. P.; Shi, Y. F.; Zhao, D. Y.; He, H. Y. *Chem. Mater.* **2006**, *18*, 3088−3095.
(15) Wang, X. Q.; Chen, M.; Huang, B.; Xu, J. C.; Peng, X. L.; Hong, B.; Jin, D. F.; Ge, H. L.; Jin, X. H. *IEEE Trans. Magn.* **2011**, *47*, 2851−2854.
(16) Yue, W.; Zhou, W. Z. *Chem. Mater.* **2007**, *19*, 2359−2363.

(17) Rumplecker, A.; Kleitz, F.; Salabas, E. L.; Schuth, F. *Chem. Mater.* **2007**, *19*, 485−496.

(18) Shu, P.; Ruan, J. F.; Gao, C. B.; Li, H. C.; Che, S. N. *Microporous Mesoporous Mater.* **2009**, *123*, 314−323.

(19) Ren, Y.; Jiao, F.; Bruce, P. G. *Microporous Mesoporous Mater.* **2009**, *121*, 90−94.

(20) Deng, J.; Zhang, L.; Dai, H.; Xia, Y.; Jiang, H.; Zhang, H.; He, H. *J. Phys. Chem. C* **2010**, *114*, 2694−2700.

(21) Yue, W. B.; Hill, A. H.; Harrison, A.; Zhou, W. Z. *Chem. Commun.* **2007**, 2518−2520.

(22) Zhao, D. Y.; Huo, Q. S.; Feng, J. L.; Chmelka, B. F.; Stucky, G. D. *J. Am. Chem. Soc.* **1998**, *120*, 6024−6036.

(23) Fan, J.; Yu, C. Z.; Gao, T.; Lei, J.; Tian, B. Z.; Wang, L. M.; Luo, Q.; Tu, B.; Zhou, W. Z.; Zhao, D. Y. *Angew. Chem., Int. Ed.* **2003**, *42*, 3146−3150.

(24) Ikedo, Y.; Sugiyama, J.; Nozaki, H.; Itahara, H.; Brewer, J. H.; Ansaldo, E. J.; Morris, G. D.; Andreica, D.; Amato, A. *Phys. Rev. B* **2007**, *75*, 054424.

(25) W.L, R. *J. Phys. Chem. Solids* **1964**, *25*, 1−10.

(26) Zeng, R.; Wang, J. Q.; Chen, Z. X.; Li, W. X.; Dou, S. X. *J. Appl. Phys.* **2011**, *109*, 07b520.

(27) Benitez, M. J.; Petracic, O.; Tüysüz, H.; Schüth, F.; Zabel, H. *EPL* **2009**, *88*, 27004.

(28) Hill, A. H.; Harrison, A.; Ritter, C.; Yue, W. B.; Zhou, W. Z. *J. Magn. Magn. Mater.* **2011**, *323*, 226−231.

(29) Fan, J.; Yu, C. Z.; Lei, J.; Zhang, Q.; Li, T. C.; Tu, B.; Zhou, W. Z.; Zhao, D. Y. *J. Am. Chem. Soc.* **2005**, *127*, 10794−10795.

(30) Yang, C. M.; Zibrowius, B.; Schmidt, W.; Schuth, F. *Chem. Mater.* **2004**, *16*, 2918−2925.

(31) Kruk, M.; Hui, C. M. *Microporous Mesoporous Mater.* **2008**, *114*, 64−73.

(32) Ersen, O.; Parmentier, J.; Solovyov, L. A.; Drillon, M.; Pham-Huu, C.; Werckmann, J.; Schultz, P. *J. Am. Chem. Soc.* **2008**, *130*, 16800−16806.

(33) Yu, T.; Zhang, H.; Yan, X. W.; Chen, Z. X.; Zou, X. D.; Oleynikov, P.; Zhao, D. Y. *J. Phys. Chem. B* **2006**, *110*, 21467−21472.

(34) Yue, W. B.; Zhou, W. Z. *J. Mater. Chem.* **2007**, *17*, 4947−4952.

(35) Kleitz, F.; Liu, D. N.; Anilkumar, G. M.; Park, I. S.; Solovyov, L. A.; Shmakov, A. N.; Ryoo, R. *J. Phys. Chem. B* **2003**, *107*, 14296−14300.

(36) Teresa, J. M. D.; Ibarra, M. R.; Algarabel, P. A.; Marquina, C.; Blasco, J.; Garcia, J.; Moral, A. d. *J. Appl. Phys.* **1997**, *81*, 5504−5504.

(37) Mousavand, T.; Naka, T.; Sato, K.; Ohara, S.; Umetsu, M.; Takami, S.; Nakane, T.; Matsushita, A.; Adschiri, T. *Phys. Rev. B* **2009**, *79*, 144411.

(38) Gangopadhyay, S.; Hadjipanayis, G. C.; Sorensen, C. M.; Klabunde, K. J. *J. Appl. Phys.* **1993**, *73*, 6964−6966.

(39) He, L.; Chen, C.; Wang, N.; Zhou, W.; Guo, L. *J. Appl. Phys.* **2007**, *102*, 103911.